IOP Publishing | International Atomic Energy Agency Nuclear Fusion
Nucl. Fusion **54** (2014) 043016 (8pp) doi:10.1088/0029-5515/54/4/043016

Stability and erosion of melt layers developed on plasma facing components of tokamaks

G. Miloshevsky and A. Hassanein

Center for Materials under Extreme Environment, School of Nuclear Engineering, Purdue University, West Lafayette, IN 47907, USA

E-mail: gennady@purdue.edu

Received 16 January 2014, revised 11 February 2014
Accepted for publication 13 February 2014
Published 18 March 2014

Abstract

Melting of metallic plasma facing components such as tungsten (W) divertor, macroscopic melt motion, and melt splashing due to edge localized modes and plasma disruptions is a major concern in fusion devices such as ITER. The viscous stability analysis and computational modelling of coupled W-melt-plasma flows are performed using the developed volume-of-fluid magnetohydrodynamic code. The effects of plasma velocity and magnetic field, whether parallel or perpendicular to the direction of W-melt flow, on melt motion and splashing from a melt pool are studied. The distributions of hydrodynamic and magnetic pressure as well as the vector fields of velocity and magnetic field are investigated. The development of waves with certain wavelengths on the W-melt surface and formation of W-melt blob on the pool's edge are observed in the absence and presence of an external magnetic field. For the investigated speeds of viscous plasma, the parallel magnetic field of 5 T does not suppress W-melt motion and splashing from the pool, plasma-induced surface waves, and ejection of molten droplets. However, the Lorentz force induced by a perpendicular magnetic field accelerates the splashing of W-melt from a melt pool but only when the stream of viscous plasma becomes well coupled to the melt motion. Under the plasma impact with high velocity of $\sim$5000 m s^{-1}, the W-melt does not undergo a significant motion disintegrating quickly into droplets dragged away by the plasma wind, independent of the presence or absence of a magnetic field. This magnitude of plasma velocity is found to be in good agreement with that predicted by the viscous stability analysis.

Keywords: melt splashing, melt pool, Lorentz force, viscous plasma

(Some figures may appear in colour only in the online journal)

1. Introduction

Tungsten (W) is currently considered as an armour material for plasma facing components (PFCs) in the ITER divertor [1]. However, during transient high heat loads from edge-localized modes (ELMs) and thermal quench disruptions, localized areas of W divertor can melt forming a melt pool on PFC surface. The macroscopic melt motion and splashing from a pool due to plasma pressure or Lorentz force can cause severe erosion and unacceptable short lifetime of PFCs [2]. Approximately 15 g of molten W was lost from the tile in the outer divertor of Alcator C-Mod during $\sim$100 discharges [3]. In the experiments carried out in the plasma edge of the TEXTOR tokamak, up to 3 g of molten W were redistributed forming mountain-like structures at the edge of the sample [4]. The ejection of molten W into the plasma core can further lead to significant plasma contamination and termination of tokamak plasma discharge [5]. A constantly present fine spray of W-melt and occasional melt splashes with continuous ligaments and large droplets is observed in TEXTOR experiments [4]. Therefore, studies and investigations of the melt behaviour in a pool under plasma impact in a strong magnetic field is a very important issue.

Plasma disruption with energy deposition of $\sim$10 MJ m^{-2} during $\sim$1 ms can result in a melt layer with depth $\sim$100–200 μm [6]. It was predicted that only a few micrometre of melt is evaporated [7, 8]. For W target exposed to a plasma impact with an energy density $\sim$30 MJ m^{-2} during $\sim$0.36 ms, W losses due to vaporization are less than $\sim$1 μm (figure 5(a) in [9]). A considerable amount of the melt layer can be swept away from the melt pool due to the melt motion under the plasma impact and external electromagnetic forces [10, 11]. The ejected molten material can accumulate at the pool's edge and splash out further resolidifying on the solid surface [12]. The formation of erosion crater and melt motion was studied using the QSPA Kh-50 plasma accelerator [13]. Large mountains of resolidified material are observed at the crater's edge. Long melt ligaments with breaking droplets at the ends were formed on the unexposed surface due to the melt outflow from the hills. It was concluded that the macroscopic motion

 © 2014 IAEA, Vienna Printed in the UK

of melt was driven by the plasma pressure gradient [13]. The formation of melt layer and its motion in the magnetic field was investigated in TEXTOR [14]. It was observed that the molten W has moved in the poloidal direction perpendicular to the magnetic field lines [15]. A deep erosion crater was developed with depth increasing poloidally up to 1 mm. A large blob of molten W was formed at the edge of W plate with two jets of width ~3 mm. These jets of molten W were splashed out on the plate within a distance of about 5 cm. The melt motion was attributed to the Lorentz force [14]. These experimental results demonstrate that the melt motion can lead to significant redistribution of PFC material during ELMs and disruptions.

In this work, the viscous stability analysis is used to study the critical velocity and growth rate of waves on the W-melt surface as a function of wavelength. The onset of instability, critical plasma velocity, development and growth of dangerous waves are predicted. The computational modelling is also performed to investigate the motion and outflow of W-melt from the melt pool. This work is an extension of our previous study on the motion and splashing of melt layers on solid substrates [16]. The impact of plasma flowing with different velocity on the development of waves on the W-melt surface is studied. The influence of a parallel or perpendicular magnetic field on the melt layer motion and splashing from a pool is investigated.

2. Theoretical and computational models

In this section we describe the viscous stability theory and volume-of-fluid magnetohydrodynamic (VoF-MHD) computational model developed to study the motion and splashing of melt layers from PFCs. The stability analysis provides an assessment of initial conditions for development and growth of surface waves, growth rates, and most dangerous wavelengths. The modelling predicts melt layer motion, plasma–melt interaction, and non-linear wave growth with ejection of molten droplets.

2.1. Viscous stability analysis

In the majority of linear stability analyses conducted with potential flow, the fluids are usually considered as inviscid [17–19]. The theory of inviscid stability of tungsten and aluminum melts and the capillary droplet-ejection model as its limiting case have been recently developed by our group [20]. However, the plasma viscosity can also affect the melt stability within a narrow boundary layer at the interface between the plasma and melt. The theory of potential flow of inviscid plasma should be replaced with that of viscous plasma. The Kelvin–Helmholtz (K–H) instability of stratified gas–liquid flow in a channel was studied by Funada and Joseph using the approach of viscous potential flow [21]. This viscous theory works well for gas–liquid flows at low Reynolds numbers, especially when the liquid layer is thin [22]. We have incorporated this viscous K–H instability analysis [21] in our problem of the plasma–melt motion and splashing. We used linearized continuity and momentum Navier–Stock equations with the assumption that the velocity can be expressed through a potential that leads to the Poisson equation. Due to this assumption, the Navier–Stock equations are completely satisfied since the viscous terms vanish, but the viscous stresses are not zero. Boundary conditions at the interface include the kinematic and dynamic conditions as well as conditions on the walls. The normal viscous stress enters into the dynamic boundary condition [21]. By applying the harmonic normal modes to the linearized Navier–Stock equations, the expressions for the relative velocity ΔV and growth rate σ_R of viscous instability are derived

$$\Delta V = |V_\mathrm{p} - V_\mathrm{m}| > \sqrt{\frac{(\mu'_\mathrm{m}+\mu'_\mathrm{p})^2}{\rho'_\mathrm{m}{\mu'_\mathrm{p}}^2+\rho'_\mathrm{p}{\mu'_\mathrm{m}}^2}\left(\frac{g(\rho_\mathrm{m}-\rho_\mathrm{p})}{k}+\gamma k\right)}, \tag{1}$$

$$\sigma_R = \pm\left(\frac{k^2(\rho'_\mathrm{m}\mu'^2_\mathrm{p}+\rho'_\mathrm{p}\mu'^2_\mathrm{m})}{(\mu'_\mathrm{m}+\mu'_\mathrm{p})^2(\rho'_\mathrm{m}+\rho'_\mathrm{p})}\Delta V^2 - \left(kg\frac{\rho_\mathrm{m}-\rho_\mathrm{p}}{\rho'_\mathrm{m}+\rho'_\mathrm{p}}+\frac{k^3\gamma}{\rho'_\mathrm{m}+\rho'_\mathrm{p}}\right)\right)^{1/2}, \tag{2}$$

where V_p, V_m, ρ_p, ρ_m denote the velocity and mass density of plasma and melt, $\rho'_\mathrm{p} = \rho_\mathrm{p}\coth(kh_\mathrm{p})$, $\rho'_\mathrm{m} = \rho_\mathrm{m}\coth(kh_\mathrm{m})$, $\mu'_\mathrm{p} = \mu_\mathrm{p}\coth(kh_\mathrm{p})$, $\mu'_\mathrm{m} = \mu_\mathrm{m}\coth(kh_\mathrm{m})$, μ_p, μ_m, h_p, h_m are the viscosity and thickness of plasma and melt, $k = 2\pi/\lambda$ is the wave number associated with small disturbances $\sim \exp(\mathrm{i}(kx+\omega t))$, λ is the wavelength, ω is the frequency, g is the gravity constant, and γ is the interfacial surface tension. The viscous plasma has significant influence on the melt stability [23]. The expressions for critical velocity (1) and growth rate (2) of viscous plasma can be reduced to those of inviscid plasma by replacing $\mu_\mathrm{p}/\mu_\mathrm{m}$ by $\rho_\mathrm{p}/\rho_\mathrm{m}$ [21]. Analysing equations (1) and (2), it can be shown that the critical velocity ΔV for viscous plasma–melt flows is always smaller than that for their inviscid counterparts [23]. It reaches a maximum when $\mu_\mathrm{p}/\mu_\mathrm{m} = \rho_\mathrm{p}/\rho_\mathrm{m}$ (an inviscid case). Therefore, the instability of melt layer can be induced by the flow of viscous plasma with significantly lower velocity.

2.2. Computational model

We briefly outline here the VoF-MHD model, details of which are given in [16]. The problems of coupled plasma–melt splashing from a pool examined in this paper are described by the incompressible Navier–Stocks equations implemented in the interFoam solver of the OpenFOAM toolbox [24]

$$\nabla\cdot\vec{u} = 0 \tag{3}$$

$$\frac{\partial\rho\vec{u}}{\partial t} + \nabla\cdot(\rho\vec{u}\vec{u}) = -\nabla p + 2\nabla\cdot(\mu\,\widehat{\tau}) + \gamma\kappa\nabla\alpha_m + \rho\,\vec{g} + \vec{J}\times\vec{B} \tag{4}$$

$$\frac{\partial\alpha_m}{\partial t} + \nabla\cdot(\alpha_m\vec{u}) + \nabla\cdot(\alpha_m(1-\alpha_m)\vec{u}_\mathrm{c}) = 0 \tag{5}$$

where $\vec{u}$ is the velocity, $\rho = \alpha_\mathrm{m}\rho_\mathrm{m} + \alpha_\mathrm{p}\rho_\mathrm{p}$ is the density with values of ρ_m and ρ_p for melt and plasma, α_m is the volume fraction of melt, $\alpha_\mathrm{p} = 1-\alpha_\mathrm{m}$ is the volume fraction of plasma, p is the pressure, $\mu = \alpha_\mathrm{m}\mu_\mathrm{m} + \alpha_\mathrm{p}\mu_\mathrm{p}$ is the viscosity with components of μ_m and μ_p for melt and plasma, $\widehat{\tau} = (\nabla\vec{u}+(\nabla\vec{u})^\mathrm{T})/2$ is the viscous stress tensor, γ is the surface tension of melt, $\kappa = -\nabla\cdot(\nabla\alpha_\mathrm{m}/|\nabla\alpha_\mathrm{m}|)$ is the curvature of the interface, $\vec{g}$ is the acceleration due to gravity, $\vec{B}$ is the magnetic field, and $\vec{J}$ is the current density. In the momentum

equation (4), the $\vec{J} \times \vec{B}$ term is absent in the original interFoam solver. The term $\rho \vec{g}$ describing the gravitational force in equation (4) can be neglected since we consider very short-length waves [18]. This computational model is based on the volume of fluid (VoF) approach [25, 26]. In the VoF method, the interface between plasma and melt is described by an indicator function defined to be the volume fraction of one of the fluids within each cell (equation (5)). The compression velocity $\vec{u}_c$ is included in equation (5) for artificial compression of the interface [26]. This extra compression contributes only in the interfacial region. Recently, this VoF model (equations (3)–(5)) was extensively validated for a variety of test cases [27].

We have implemented both the thermal conduction and magnetic induction equations in the basic VoF algorithm (equations (3)–(5)). The heat conduction equation coupling the velocity–temperature field and the magnetic induction equation describing the evolution of a magnetic field are given as

$$\frac{\partial \rho c_p T}{\partial t} + \nabla \cdot (\rho c_p \vec{u} T) = \nabla \cdot (k \nabla T) + Q_J \quad (6)$$

$$\frac{\partial \vec{B}}{\partial t} + \nabla \cdot (\vec{u}\vec{B} - \vec{B}\vec{u}) - \nabla \cdot \frac{\nabla \vec{B}}{\sigma \mu} = 0 \quad (7)$$

where T is the temperature, $c_p = \alpha_m c_{pm} + \alpha_p c_{pp}$ and $k = \alpha_m k_m + \alpha_p k_p$ are respectively the specific heat capacity at constant pressure and the thermal conductivity assuming the values c_{pm}, k_m and c_{pp}, k_p for melt and plasma, $Q_J = \vec{J} \cdot \vec{J}/\sigma$ is the Joule heating due to the electric current, $\sigma = \alpha_m \sigma_m + \alpha_p \sigma_p$ is the electric conductivity with values of σ_m and σ_p for melt and plasma, μ is the magnetic permeability. The heat equation (6) includes a source term Q_J due to the Joule heating. The magnetic field $\vec{B}$ is calculated by solving the induction equation (7) and then used to calculate the electric current as $\vec{J} = (\nabla \times \vec{B})/\mu$. We note that the current $\vec{J}$ is the induced current due to variations in the magnetic field. The calculated $\vec{B}$ and $\vec{J}$ are used to compute the Lorentz force $\vec{J} \times \vec{B} = -\nabla B^2/(2\mu) + \vec{B}\nabla\vec{B}/\mu$ and Joule heating Q_J. The Lorentz force $\vec{J} \times \vec{B}$ expressed through the magnetic pressure (first term) and magnetic tension (second term) is included in the momentum equation (4). In the VoF model, single fields of velocity, pressure, temperature, and magnetic field are defined for both plasma and melt. Volume fractions, densities, viscosities, specific heat capacities, thermal and electrical conductivities are defined individually for each of fluids. The implementation of equations (6) and (7) in the interFoam solver is made using top-level syntax of natural OpenFOAM language of equation mimicking. The Shercliff and Hunts problems [28, 29] were used for the VoF-MHD model to benchmark the liquid metal flow in a rectangular duct under an externally applied magnetic field. The VoF-MHD model was also validated for the case of a single bubble rising in a liquid metal under imposed vertical magnetic field [30]. The resulting VoF-MHD solver is then used for the modelling of coupled plasma–melt motion and splashing from a pool without/with the applied external magnetic field.

3. Results and discussion

In this section the theoretical results from the viscous stability analysis on the onset conditions for development and growth of surface waves at the interface between plasma and W-melt are presented. The results of computational modelling on the melt motion and splashing from a pool, the impact of plasma stream with different velocity on the W-melt surface, and the effects of a magnetic field on W-melt motion are illustrated. For moderate plasma velocities ($\leqslant$1000 m s^{-1}), the computational results are shown for a time period ~1 ms that is an overlap between the duration of ELMs (~0.1–1.0 ms) and plasma disruptions (~1–10 ms) [31].

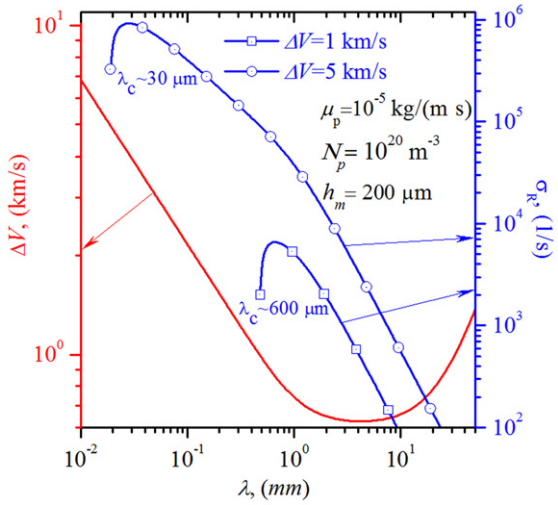

Figure 1. Relative velocity (solid curve) and growth rates (solid curves with symbols) of waves on W-melt surface as a function of wavelength.

3.1. Critical velocity and growth rate of surface waves

The onset of viscous instability is analytically studied using equations (1) and (2). In this analysis, it is assumed that the W-melt moves with velocity of ~2 m s^{-1}. The density of W-melt is $\rho_m = 16400$ kg m^{-3}. W-melt thickness is ~ 200 μm. The dynamic viscosity is $\mu_m \sim 7 \times 10^{-3}$ kg m^{-1} s^{-1}. The surface tension of W-melt is $\gamma = 2.48$ N m^{-1}. The gravity constant is 9.81 m s^{-2}. The velocity of hydrogen plasma flowing over the W-melt surface was ranged from 0 to 5000 m s^{-1}. The number density of plasma is ~ 10^{20} m^{-3} ($\rho_p \sim 1.67 \times 10^{-7}$ kg m^{-3}) that is relevant to ITER conditions. The dynamic viscosity of plasma is 10^{-5} kg m^{-1} s^{-1}. The relative velocity ΔV and growth rate σ_R as a function of wavelength λ are shown in figure 1. The growth rates are illustrated for plasma velocities of 1000 and 5000 m s^{-1}. The arrows in figure 1 indicate the axis to which curve belongs to. The unstable region is located above the ΔV curve. The growing waves with critical wavelengths of ~3–8 mm can be generated by a plasma streaming with velocity higher than ~600 m s^{-1}. However, the wavelength of these waves are more than an order of magnitude larger compared to the thickness of melt layer, ~0.2 mm. The growth of these large waves on a thin melt layer may not occur. For a plasma flowing with ~1000 m s^{-1}, the fastest growing wavelength is ~600 μm (figure 1). This is still about three times larger than the melt thickness of ~200 μm. The characteristic time ~$1/\sigma_R$ estimated from the growth rate is about ~0.2 ms (curve with square symbols). The flow of plasma with velocity of ~5000 m s^{-1} generates the surface

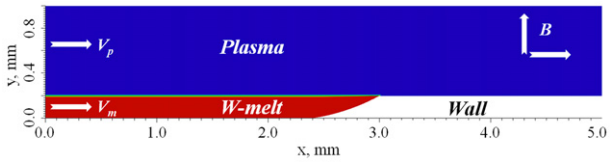

Figure 2. Computational domain used in modelling W-melt motion and splashing from melt pool.

waves with the fastest growing 'dangerous' wavelength on the order of ∼30 μm (curve with circles). The wavelength of these short waves is smaller than the thickness of W-melt, and the ejection of droplets is then expected from the W-melt surface. The characteristic timescale of droplet development estimated from the growth rate curve is on the order of ∼1 μs.

3.2. Computational domain and numerical set-up

A computational domain in 2D geometry ($(x,\ y)$-plane) is illustrated in figure 2. The domain's length is 5 mm and the height is 1 mm. The interface between W-melt and plasma is at $y = 200\,\mu$m. The W-melt is confined in a pool with the length of 3 mm and the depth of 200 μm. It was noted in [18] that for the modelling of viscous flows the periodic boundary conditions are not appropriate due to viscous dissipation at the interface and on the walls. The computational domain should include the inlet and outlet for W-melt and plasma. The simulations involving the boundary conditions with inlet and outlet were recently carried out for viscous W-melt-plasma flows [23]. Therefore, the velocities of W-melt $V_{\rm m}$ and plasma $V_{\rm p}$ are set to specified values at the inlet on the left-hand side of the computational domain.

The boundary condition for pressure at the inlet is zero gradient. At the outlet on the right-hand side of domain, the pressure is fixed to a background value. The boundary condition for velocity is zero gradient. At bottom wall, the non-slip boundary condition is used for velocity with zero gradient for pressure. The top of domain is a free boundary with both outflow and inflow of plasma. The parameters and physical properties of W-melt and plasma used in the modelling can be found in [23]. We shortly describe some of the parameters needed in this pool-specific modelling. The stationary velocity of melt motion estimated in TEXTOR experiments was about 1.7 m s^{-1} [32]. Therefore, we set the velocity of W-melt to $V_{\rm m} \sim 2\,{\rm m\,s^{-1}}$. The velocity of plasma during ELMs and disruptions is uncertain. The ELM plasma velocity in the DIII-D tokamak is found to be ∼0.5 km s^{-1} in the poloidal direction and ∼10–20 km s^{-1} in the toroidal direction [33]. Plasma streams with velocities higher than ∼100–400 km s^{-1} can be produced in plasma compressors and accelerators [34, 35]. Therefore, the modelling is performed for three velocities of hydrogen plasma $V_{\rm p} \sim 100\,{\rm m\,s^{-1}}$, ∼1000 m s^{-1} and ∼5000 m s^{-1}, respectively. It is found in the recent computational study that there is a strong influence of plasma speed on the stability of W-melt layer [16]. At ∼5000 m s^{-1} and higher velocities, the instability of W-melt and droplet ejection is predicted from the viscous stability analysis (section 3.1). The externally imposed magnetic field is $B = 5\,{\rm T}$. The estimated magnetic Reynolds number [16] is small for both W-melt and plasma ($Rem_{\rm m} \sim 0.08$, $Rem_{\rm p} \sim 0.0002$–0.02) meaning that the induced magnetic field is negligible compared to the imposed magnetic field. Therefore, the magnetic tension term in the expression for the Lorentz force (section 2.2) can be neglected since $\nabla\vec{B}$ is very close to zero. The main contribution to the Lorentz force comes from the magnetic pressure. The simulation is carried out for three cases: (1) no magnetic field; (2) magnetic field is parallel to the flow direction; and (3) magnetic field is perpendicular to the flow direction (figure 2).

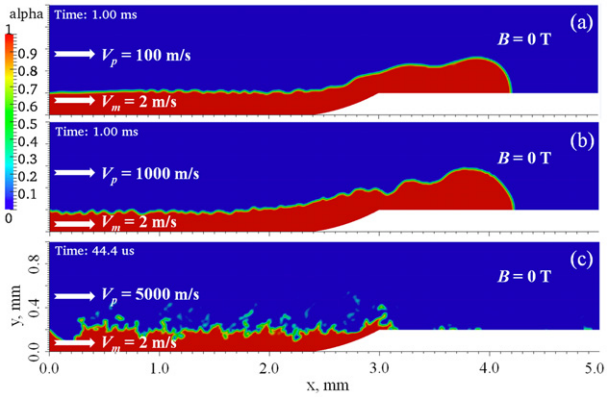

Figure 3. Volume fraction (alpha) of W-melt for specified time moments in the absence of magnetic field effects. The velocity of plasma is (*a*) 100 m s^{-1}; (*b*) 1000 m s^{-1}; and (*c*) 5000 m s^{-1}. The velocity of W-melt is 2 m s^{-1}.

3.3. Motion and splashing of W-melt from a melt pool in the absence of a magnetic field

The fields of volume fraction of W-melt and plasma are shown in figure 3. For this particular case, the influence of the magnetic field on W-melt motion is not considered. The W-melt moves with speed of 2 m s^{-1}. The plasma velocity is 100 m s^{-1} (figure 3(*a*)), 1000 m s^{-1} (figure 3(*b*)), and 5000 m s^{-1} (figure 3(*c*)), respectively. At $t = 0$, the W-melt with an unperturbed interface is initially located in the pool formed due to an ELM or a disruption (figure 2). As time progresses, the coupled flow of W-melt and plasma streamlines in the x-direction. The interaction between plasma and melt results in the generation of surface waves due to the shear force exerted by the plasma. The snapshots of W-melt/plasma interface are illustrated for time moments of 1 ms (figures 3(*a*) and (*b*)) and 44.4 μs (figure 3(*c*)). It is observed that depending on the speed of plasma the effect of plasma on the melt motion is quite different [16]. For plasma flowing with velocities of 100 and 1000 m s^{-1}, wavy structure is generated on the melt surface. Due to the melt motion and splashing from the pool, a large blob of W-melt with a maximum height of ∼400 μm develops on the pool's edge. This kind of hill structures or leading edges with heights of several mm were reported in TEXTOR experiments [4]. The front of the blob is steep enough because of the non-slip boundary condition at the bottom wall.

Further, the blob of W-melt displaces on the solid surface due to the melt inflow. It can be seen that the displaced melt moved about ∼1.2 mm during ∼1 ms (figures 3(*a*) and (*b*)). A large wave develops on the blob near the pool edge. The distance of blob movement is nearly the same for plasma

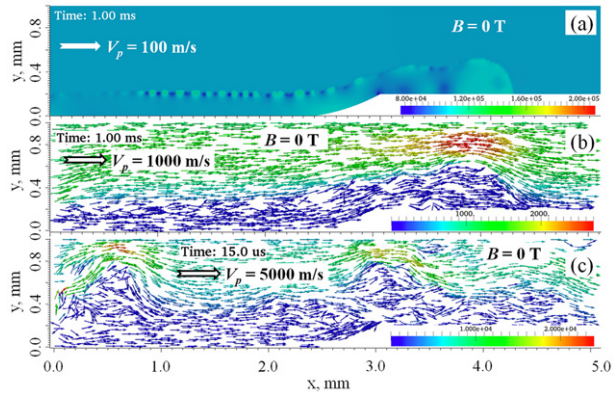

Figure 4. Map of pressure (*a*) and vector fields of velocity for plasma flowing with speed of 1000 m s^{-1} (*b*) and 5000 m s^{-1} (*c*) in absence of magnetic field. In panel (*a*), the pressure in legend is in units of Pa. In panels (*b*) and (*c*), the units of velocity in legend are in m s^{-1}.

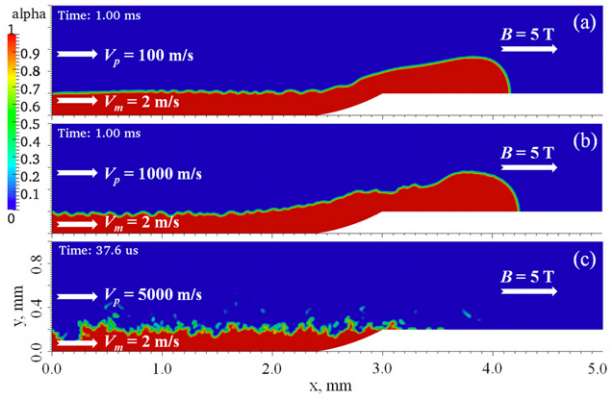

Figure 5. Volume fraction (alpha) of W-melt for specified time moments in the presence of a magnetic field of 5 T parallel to the direction of plasma–melt flow. The velocity of plasma is (*a*) 100 m s^{-1}; (*b*) 1000 m s^{-1}; and (*c*) 5000 m s^{-1}. The velocity of W-melt is 2 m s^{-1}.

flow with velocity of 100 m s^{-1} and 1000 m s^{-1}. Thus, it can be concluded that the plasma stream with velocity $V_p \leqslant 1000$ m s^{-1} has little influence on melt motion. Surface waves with shorter wavelengths are generated on the melt surface as the speed of plasma increases. For plasma streaming with speed of 5000 m s^{-1}, the W-melt disintegrates into droplets in less than 0.1 ms (figure 3(*c*)). The melt as a whole undergoes only insignificant movement during this short time. Thus, there is a strong impact of plasma flow on the behaviour of W-melt in this case. Fine droplets are stripped and ejected from the W-melt surface and dragged away by a plasma wind. Small plasma bubbles are entrained and mixed with the melt. The topological structure of the interface is very complex. The ejected molten droplets that have fallen and redeposited on the solid surface can be seen in figure 3(*c*).

The maps of the pressure and vector fields of velocity are shown in figure 4. The pressure distribution is illustrated at time 1 ms for the case of plasma flowing with velocity of 100 m s^{-1} (figure 3(*a*)). The background pressure is 10^5 Pa. Variations of pressure are seen at the W-melt-plasma interface as well as within a melt blob (figure 4(*a*)). High and low pressure regions are alternately formed at wave crests and troughs, respectively. The pressure is higher near the edge of pool (from 2 to 3 mm) and in some regions of melt blob. The zones of low pressure are seen within a melt blob near the solid surface (at 3.0 and 3.6 mm). The melt surface is generally depressed in regions of high pressure, whereas the interface is rising in areas of low pressure.

These pressure fluctuations create waves with various wavelengths that propagate on the melt surface in the direction of plasma flow. Depending on the relative plasma–melt speeds and local pressure fluctuations, the generation of waves with different wavelengths occurs. Thus, the melt surface is composed of waves with various amplitudes, frequencies, and wavelengths. The interaction among these waves results in the formation of surface waves with an 'average' wavelength. There is also strong coupling between the plasma flow and the motion of waves. In addition to the mentioned effect of plasma on W-melt, the disturbances in the melt surface (waveforms) induce perturbations in the plasma flow. The boundary layer is formed with vortex structures developed at the plasma–melt interface (figures 4(*b*) and (*c*)). The velocity decreases from the bulk plasma value (1000 and 5000 m s^{-1}) to that of the melt motion (2 m s^{-1}) within this thin layer. In some regions, the local velocity of plasma stream is about 3–4 times higher compared to the background velocity. For high-speed plasma flow (figure 4(*c*)), the complex vorticity and swirling flows in the boundary layer are responsible for the growth of short length waves, ejection of droplets, and melt disintegration.

3.4. Motion and splashing of W-melt from a melt pool in the presence of a parallel magnetic field

In this section, the influence of a parallel magnetic field of 5 T to the direction of plasma–melt flow is taken into account. The simulation conditions are similar to those of figure 3. The volume fraction of W-melt is shown in figure 5.

It can be seen that a magnetic field parallel to the direction of W-melt motion has little effects on development of melt blob on the edge of pool and generation of surface waves on the melt. This is because the Lorentz force does not affect the melt motion either in the positive or negative x-direction. It acts perpendicularly to the W-melt layer. Therefore, the effect of electromagnetic forces on the melt motion is insignificant in this case. It can also be seen in figures 5(*a*) and (*b*) that during ~1 ms the location of melt blob is nearly the same as that found in the absence of magnetic field effects (figures 3(*a*) and (*b*)). The height of W-melt swept away from the melt pool is ~300–400 μm. The waves on the melt surface are produced by the plasma stream. It is observed that the time-course and waveform structure of waves is the same in the absence and presence of a parallel magnetic field.

For plasma streaming with velocity of 100 m s^{-1} (figures 3(*a*) and 5(*a*)), the development of surface waves begins near the edge of pool in the region from 2 to 2.5 mm. As W-melt splashes out of pool forming a melt blob, these waves with short wavelengths (~0.1 mm) propagate in the backward direction toward the inlet. At time ~1 ms, portion of the melt layer (~0.8 mm) near the inlet still remains flat (figures 3(*a*) and 5(*a*)). At later time ~1.4 ms, the melt surface in the pool is entirely covered by waves (results not shown). Shortly after that, the waves with longer wavelengths start to

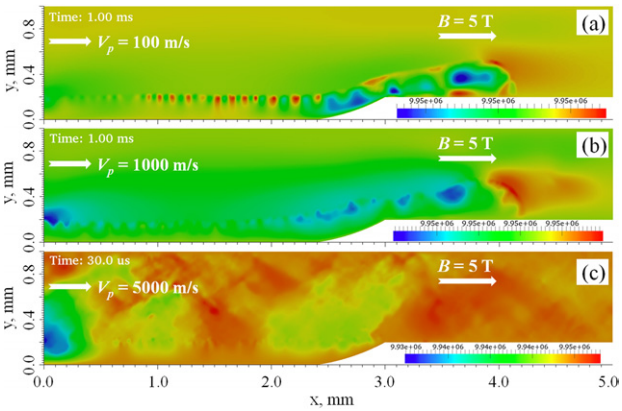

Figure 6. Maps of magnetic pressure for plasma flowing with velocity of 100 m s^{-1} (*a*), 1000 m s^{-1} (*b*) and 5000 m s^{-1} (*c*). The 5 T magnetic field is parallel to the direction of W-melt-plasma flow. In legends, the pressure is expressed in units of Pa.

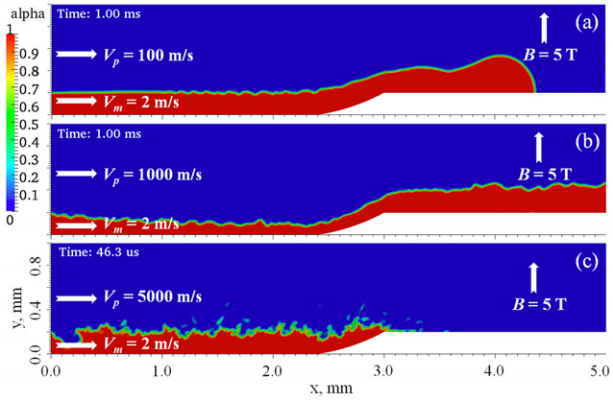

Figure 7. Volume fraction (alpha) of W-melt for specified time moments in the presence of 5 T magnetic field perpendicular to the direction of plasma–melt flow. The velocity of plasma is (*a*) 100 m s^{-1}; (*b*) 1000 m s^{-1}; and (*c*) 5000 m s^{-1}. The velocity of W-melt is 2 m s^{-1}.

run downstream from the inlet in the forward direction. The melt blob leaves the computational domain through the outlet at time ∼1.65 ms. Later after ∼3 ms, the steady flow of W-melt is then established with characteristic wavelength is on the order of ∼0.2 mm.

For plasma flowing with velocity of 1000 m s^{-1} (figures 3(*b*) and 5(*b*)), the observed dynamics of wave development is quite different from the previous case. A single wave with growing wavelength (∼0.1–0.2 mm) is shortly induced during ∼0.02 ms near the inlet by the plasma flow. This wave propagates quickly on melt surface in the forward direction. A train of waves with shorter wavelengths is generated behind this single wave. At time ∼0.2 ms, this structure of waves travels about ∼1 mm. At this time, the melt blob is formed and the other structure of waves starts to develop near the edge of pool. These waves move in the backward direction. At ∼0.4 ms, the two systems of waves collide. At later times, the waves running in the forward direction only survive. At time ∼1 ms (figures 3(*b*) and 5(*b*)), the wavy structure on the W-melt surface with wavelength on the order of ∼0.1 mm is well developed. The melt blob is located at ∼4.2 mm.

For high-speed plasma streaming with velocity of 5000 m s^{-1}, a large melt disturbance develops during ∼5 μs near the inlet. At ∼10 μs, first molten droplets are ejected. At time ∼15 μs, the small ripples with very short wavelengths start to develop and grow near the edge of pool in the region from 2.4 mm to 3 mm (figure 5(*c*)). At ∼30 μs, the surface of W-melt is completely covered by wavy ripples with ejection of droplets near the inlet and edge of pool. At later times, the droplets are ejected from the entire melt surface (figures 3(*c*) and 5(*c*)) moving in the direction of plasma flow that is in agreement with observations in ASDEX Upgrade experiments [5]. During this short timescale ∼40–50 μs, the W-melt layer initially located in the pool does not undergo significant motion or splashing at the pool's edge. Thus, we conclude that the magnetic field of 5 T that is parallel to a melt layer does not suppress the W-melt motion, plasma-induced development of surface waves, or the ejection of droplets.

The map of magnetic pressure is shown in figure 6. For a magnetic field of 5 T, an estimate of magnetic pressure is $p_m = B^2/(2\mu) \approx 9.95 \times 10^6$ Pa. This is about two orders of magnitude larger than the background hydrodynamic pressure $p \approx 1.0 \times 10^5$ Pa. It can be seen in figure 6 that the gradients of magnetic pressure are extremely small. For plasma flow with velocity of 100 m s^{-1} and 1000 m s^{-1} (figures 6(*a*) and (*b*)), the difference is negligible. The magnetic pressure is mainly varied at the interface between W-melt and plasma, within a melt blob, and near a solid wall at the edge of pool. The magnetic pressure is also larger in the vicinity of the front of melt blob. For plasma streaming with speed of 5000 m s^{-1}, the disturbance of magnetic pressure is seen within a wide area (figure 6(*c*)). However, the variation of magnetic pressure is still insignificant. These small variations mean that the pressure gradients due to a magnetic field are negligible. The reason is that the changes of a magnetic field due to the W-melt-plasma motion are very small as will be shown next later. Thus, we conclude that flow variations are mainly induced by the hydrodynamic pressure.

3.5. Motion and splashing of W-melt from a melt pool in the presence of perpendicular magnetic field

The direction of the magnetic field is assumed perpendicular to the W-melt layer. In this case, the Lorentz force may act either along or against the direction of the W-melt-plasma flow, thus affecting its behaviour. The results on the volume fraction of W-melt are shown in figures 7(*a*) and (*b*) at time ∼1 ms for a plasma flowing with velocity of 100 m s^{-1} and 1000 m s^{-1}, respectively. The topological structure of the W-melt surface is illustrated in figure 7(*c*) at time ∼46.3 μs for a plasma streaming with velocity of 5000 m s^{-1}. In the case of plasma flow with velocity of 100 m s^{-1} (figure 7(*a*)), there is little change in the volume fraction of W-melt compared to the cases shown in figures 3(*a*) and 5(*a*). The dynamics of melt motion, wave development, and formation of melt blob in a perpendicular magnetic field is similar to that described in section 3.4. However, it is seen in figure 7(*a*) that at time ∼1 ms the front of melt blob is more advanced by ∼0.2 mm and the length of the flat melt region near the inlet unperturbed by waves is about ∼1 mm. Thus, during ∼1 ms the impact of plasma with velocity of 100 m s^{-1} on W-melt is not significant.

At this plasma speed, time ∼1 ms is short enough for the wavy structure on the W-melt surface to become well developed. As discussed in section 3.4, plasma flowing with velocity of 1000 m s^{-1} over W-melt during ∼1 ms generates well-developed wavy structure. Thus, during this time interval the flow of plasma is well coupled to the flow of W-melt. A perpendicular magnetic field of 5 T has a significant influence on the W-melt motion. Due to the Lorentz force affecting the coupled W-melt-plasma flow, the dynamics of W-melt (figure 7(*b*)) is completely different compared to that shown in figures 3(*b*) and 5(*b*) and described in section 3.4.

As in the previous cases, a single W-melt wave is initially induced by the plasma flow near the inlet. However, it travels faster reaching ∼1 mm during ∼0.18 ms. At time ∼0.3 ms, the waves are developed on the entire surface of W-melt. The melt blob is not formed at the edge of pool, but the W-melt layer with height ∼200 μm and abrupt front moves on the solid substrate. The thickness of W-melt in the pool starts to fluctuate with a large wavelength of ∼0.5–1.0 mm. The front of W-melt reaches a location of ∼4.2 mm at time ∼0.55 ms. This is almost two times faster compared to the cases shown in figures 3(*b*) and 5(*b*). The front of melt is deformed with a spike of ∼0.2 mm and height ∼100 μm protruded forward on the solid substrate. At later times, the length of this melt spike increases and large wavy structures develop on the melt front. The W-melt reaches the right side of the computational domain at time ∼0.8 ms. In previous cases (figures 3(*b*) and 5(*b*)), this happens at time ∼1.5 ms. After that, W-melt moves out through the outlet. It is seen in figure 7(*b*) that at time ∼1 ms the thickness of melt is about ∼200 μm on the substrate outside the pool, but the W-melt is thinner inside the pool. We conclude that the coupled flow of W-melt and plasma is accelerated in the magnetic field perpendicular to the direction of their motion. For plasma streaming with velocity of 5000 m s^{-1} (figure 7(*c*)), the surface of W-melt becomes disturbed during tens of microseconds due to plasma impact. As in previous cases (figures 3(*c*) and 5(*c*)), the waves with very short wavelengths grow quickly on the W-melt surface breaking-up and ejecting droplets into the plasma. The melt does not undergo significant motion during this short time. Thus, at high plasma speeds ∼5000 m s^{-1} no influence is predicted of a perpendicular magnetic field on melt layer stabilization.

The fluctuations of a magnetic field that is parallel or perpendicular to the direction of coupled W-melt-plasma flow are illustrated in figure 8 for time ∼35 μs. It can be seen that compared to the externally imposed field of 5 T, the local disturbance of a magnetic field (induced field) due to the motion of W-melt and plasma is very small. In legends, the change is seen in a third digit after comma. The reason is that the magnetic Reynolds number is small for both W-melt and plasma indicating the effects of magnetic advection are relatively unimportant.

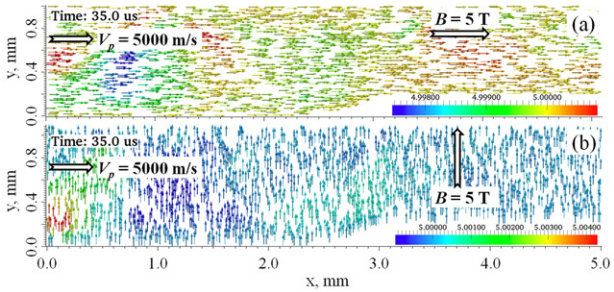

Figure 8. Maps of magnetic field at time ∼35 μs for plasma flowing with velocity of 5000 m s^{-1} in the presence of magnetic field that is (*a*) parallel and (*b*) perpendicular to W-melt layer. In legends, the magnetic field is expressed in units of T.

4. Conclusions

The viscous stability theory is developed and applied to investigate the stability of W-melt in a melt pool under the impact of viscous plasma. The onset conditions of viscous instability, most dangerous wavelengths, and growth rates are predicted for ITER-like conditions. It is found that the viscous plasma streaming over W-melt surface with velocity of ⩾5000 m s^{-1} can produce melt disturbances with the fastest growing wavelength on the order of ∼30 μm. This wavelength is smaller than a typical thickness of melt layer ∼100–200 μm. These short waves can then grow on the timescale of ∼1 μs.

The VoF-MHD computational model is developed and implemented in the framework of OpenFOAM package. The developed VoF-MHD code is then used to study the motion and splashing of W-melt from a melt pool on PFCs. In the absence of a magnetic field, it is observed that plasma streaming with velocity of ⩽1000 m s^{-1} has little effect on melt motion and splashing from a pool. During ∼1 ms, waves are generated on the W-melt surface and large blob of W-melt is formed on the pool's edge within ∼1.2 mm. Plasma streaming with velocity of ∼5000 m s^{-1} has strong impact on the behaviour of W-melt. W-melt becomes disintegrated into droplets in less than 0.1 ms without significant movement and splashing from a pool. Droplets are stripped from W-melt and dragged away by the incident plasma wind.

The presence of a magnetic field that is parallel to the direction of W-melt motion has no significant effect on generation of waves on melt surface and on formation of melt blob on pool's edge. For all three considered plasma speeds, waveforms and time-course of wave development are very similar to those in the absence of a magnetic field. However, the magnetic field perpendicular to the direction of W-melt motion produces Lorentz force that significantly affects melt splashing from pool when the flow of plasma with velocity of ∼1000 m s^{-1} becomes well coupled to the flow of W-melt. For lower plasma speeds ∼100 m s^{-1}, the melt acceleration is insignificant. At high plasma speeds ∼5000 m s^{-1}, the W-melt disintegrates into droplets before it even moves. Therefore, we conclude that there is a certain regime when the flows of W-melt and plasma in a perpendicular magnetic field become well coupled and accelerated by the Lorentz force resulting in a large redistribution and disintegration of W-melt. This is a very serious concern for PFC lifetime as well as plasma contamination and reliable operation.

Acknowledgment

This work is supported by the US Department of Energy, Office of Fusion Energy Sciences.

References

[1] Hirooka Y. *et al* 1992 Evaluation of tungsten as a plasma-facing material for steady-state magnetic fusion devices *J. Nucl. Mater.* **196** 149

[2] Roth J. *et al* 2009 Recent analysis of key plasma wall interactions issues for ITER *J. Nucl. Mater.* **390–391** 1

[3] Lipschultz B. *et al* 2012 Divertor tungsten tile melting and its effect on core plasma performance *Nucl. Fusion* **52** 123002

[4] Coenen J.W. *et al* 2011 Analysis of tungsten melt-layer motion and splashing under tokamak conditions at TEXTOR *Nucl. Fusion* **51** 083008

[5] Krieger K. *et al* 2011 Induced tungsten melting events in the divertor of ASDEX Upgrade and their influence on plasma performance *J. Nucl. Mater.* **415** S297

[6] Hassanein A. *et al* 2009 Integrated simulation of plasma surface interaction during edge localized modes and disruptions: self-consistent approach *J. Nucl. Mater.* **390–391** 777

[7] Hassanein A. and Konkashbaev I. 1996 Lifetime evaluation of plasma-facing materials during a tokamak disruption *J. Nucl. Mater.* **233** 713

[8] Hassanein A. and Konkashbaev I. 1999 Comprehensive physical models and simulation package for plasma/material interactions during plasma instabilities *J. Nucl. Mater.* **273** 326

[9] Shi Y. *et al* 2011 Boiling induced macroscopic erosion of plasma facing components in fusion devices *Fusion Eng. Des.* **86** 155

[10] Wurz H. *et al* 2001 Macroscopic erosion in tokamak off normal events *Fusion Eng. Des.* **56–57** 397

[11] Garkusha I.E. *et al* 2007 Tungsten melt layer erosion due to $J \times B$ force under conditions relevant to ITER ELMs *J. Nucl. Mater.* **363** 1021

[12] Dale G.E. and Bourham M.A. 1998 Melt layer erosion and resolidification of metallic plasma facing components *17th IEEE/NPSS Symp. (San Diego, 6–10 October 1997) Fusion Eng.* **2** 892–95

[13] Tereshin V.I. *et al* 2003 Influence of plasma pressure gradient on melt layer macroscopic erosion of metal targets in disruption simulation experiments *J. Nucl. Mater.* **313** 685

[14] Sergienko G. *et al* 2007 Experience with bulk tungsten test-limiters under high heat loads: melting and melt layer propagation *Phys. Scr.* **T128** 81

[15] Sergienko G. *et al* 2007 Erosion of a tungsten limiter under high heat flux in TEXTOR *J. Nucl. Mater.* **363** 96

[16] Miloshevsky G. and Hassanein A. 2014 Effects of plasma flow velocity on melt-layer splashing and erosion during plasma instabilities *Nucl. Fusion* **54** 033008

[17] Chandrasekhar S. 1961 *Hydrodynamic and Hydromagnetic Stability* (London: Oxford University Press)

[18] Miloshevsky G.V. and Hassanein A. 2010 Modelling of Kelvin–Helmholtz instability and splashing of melt layers from plasma-facing components in tokamaks under plasma impact *Nucl. Fusion* **50** 115005

[19] Miloshevsky G. and Hassanein A. 2011 Modeling of macroscopic melt layer splashing during plasma instabilities *J. Nucl. Mater.* **415** S74

[20] Shi Y. *et al* 2011 Theoretical studies of macroscopic erosion mechanisms of melt layers developed on plasma facing components *J. Nucl. Mater.* **412** 123

[21] Funada T. and Joseph D.D. 2001 Viscous potential flow analysis of Kelvin–Helmholtz instability in a channel *J. Fluid Mech.* **445** 263

[22] Adhamkhodaparast K. *et al* 1995 The Rayleigh–Taylor and Kelvin–Helmholtz stability of a viscous liquid–vapor interface with heat and mass-transfer *Phys. Fluids* **7** 359

[23] Miloshevsky G. and Hassanein A. 2013 Splashing and boiling mechanisms of melt layer losses of PFCs during plasma instabilities *J. Nucl. Mater.* **438** S155

[24] OpenFOAM (2013), user guide, version 2.2.2 Available from: www.openfoam.org

[25] Hirt C.W. and Nichols B.D. 1981 Volume of fluid (Vof) method for the dynamics of free boundaries *J. Comput. Phys.* **39** 201

[26] Berberovic E. *et al* 2009 Drop impact onto a liquid layer of finite thickness: dynamics of the cavity evolution *Phys. Rev.* E **79** 036306

[27] Deshpande S.S. *et al* 2012 Evaluating the performance of the two-phase flow solver interFoam *Comput. Sci. Discovery* **5** 014016

[28] Shercliff J.A. 1953 Steady motion of conducting fluids in pipes under transverse magnetic fields *Math. Proc. Camb. Philos. Soc.* **49** 136

[29] Hunt J.C.R. 1965 Magnetohydrodynamic flow in rectangular ducts *J. Fluid. Mech.* **21** 577

[30] Shibasaki Y. *et al* 2010 Computation of a rising bubble in an enclosure filled with liquid metal under vertical magnetic fields *ISIJ Int.* **50** 363

[31] Federici G. *et al* 2001 Plasma–material interactions in current tokamaks and their implications for next step fusion reactors *Nucl. Fusion* **41** 1967

[32] Sergienko G. *et al* 2005 Tungsten melting under high power load in the TEXTOR edge plasma *32nd EPS Conf. on Plasma Physics and Controlled Fusion (Tarragona, Spain, 2005)* vol 29C (ECA) P-1.019

[33] Boedo J.A. *et al* 2005 Edge-localized mode dynamics and transport in the scrape-off layer of the DIII-D tokamak *Phys. Plasmas* **12** 072516

[34] Dojcinovic I.P. 2010 Plasma flow interaction with ITER divertor related surfaces *J. Phys.: Conf. Ser.* **257** 012033

[35] Tereshin V.I. 1995 Quasi-stationary plasma accelerators (QSPA) and their applications *Plasma Phys. Control. Fusion* **37** A177